Journal of Applied Physics ARTICLE pubs.aip.org/aip/jap

Demonstrating resonant ultrasound spectroscopy as a viable technique to characterize thermally conditioned high explosive materials

Cite as: J. Appl. Phys. **135**, 035103 (2024); doi: 10.1063/5.0189958
Submitted: 1 December 2023 · Accepted: 28 December 2023 ·
Published Online: 18 January 2024

Jordan S. Lum,[a] David M. Stobbe, Paul B. Mirkarimi, William L. Shaw, Henry E. Reinstein, Rebecca K. Lindsey,[b] and Richard H. Gee

AFFILIATIONS

Lawrence Livermore National Laboratory, Livermore, California 94550, USA

[a]**Author to whom correspondence should be addressed:** Lum21@llnl.gov
[b]**Present address:** Department of Chemical Engineering, University of Michigan, Ann Arbor, MI 48109, USA.

ABSTRACT

We present results of resonant ultrasound spectroscopy (RUS) measurements applied to granular high explosive materials at different bulk pressing densities and degree of thermal conditioning. The material chosen in this study is a ubiquitously used explosive material known as pentaerythritol tetranitrate (PETN), which is used commercially in civil and defense applications both as a binderized plastic bonded explosive material and an unbinderized neat material. However, changes in granular PETN bulk elastic properties due to thermal conditioning, which could have implications for better understanding environmental aging-related effects, have not been well studied even though it is believed that elasticity may play an important role in explosive material initiation mechanisms. Furthermore, monitoring elastic property changes in granular explosive pressings has not yet been demonstrated using RUS, which is an appealing non-destructive characterization tool that requires only dry point contact with the explosive material. To this end, we report the first study using RUS to quantify the elastic properties of binderized and neat PETN pressings as well as to quantify changes in elastic properties as a function of both thermal conditioning and bulk pressing density. Elastic stiffness coefficients, sometimes more commonly referred to as elastic constants, calculated from the RUS measurements on the different PETN-based materials show a significant increase for the post-conditioned samples compared to the pre-conditioned samples. This trend of increasing elastic properties with thermal conditioning was consistent for different density pressings, different thermal exposure conditions, and even different neat PETN pressings of differing average crystal sizes and/or specific surface areas.

I. INTRODUCTION

Resonant ultrasound spectroscopy (RUS) is a non-destructive characterization technique that can be used to quantify the elastic properties of materials.[1] This involves exciting and measuring the natural frequencies (i.e., normal modes) of an object, which, along with the object's outer dimensions, density, and an initial guess of the elastic stiffness coefficients, can be used in an inversion model to calculate the object's elastic properties.[1–3] One advantage of this technique over traditional time-of-flight ultrasound measurements is that lower order symmetry materials can be fully characterized. Moreover, it does not require a couplant, which can be attractive for some materials since (1) chemical compatibility tests are sometimes required for any new couplant-material combinations and (2) the couplant residue cannot always be removed from samples, resulting in a destructive measurement. These advantages of using RUS as a characterization tool are found to be especially beneficial when inspecting granular materials, such as high explosives (HEs).

Granular and plastic bonded high explosive materials, such as pentaerythritol tetranitrate (PETN) based materials, are commonly used for a myriad of civil and defense applications.[4] It is generally believed that HE performance for these applications can be greatly impacted by changes in the material crystal size and shape.[5–8] For example, organic granular high explosives have been shown to

exhibit changes in sensitivity over time due to thermally induced changes, e.g., to a material microstructure due to mass transport and redistribution.[5,6,9–13] These changes can be detected using atomic force microscopy,[14–16] optical microscopy,[17] or a Fisher sub-sieve sizer;[6–8] however, these techniques only provide an understanding of microstructure and not mechanical properties of the material, which may also play an important role in HE performance.[18]

Recently, a *nonlinear* resonant ultrasound technique capable of probing HE nonlinear mechanical properties was proposed[19] for predicting sensitivity to initiation in granular high explosives. In this approach, resonant frequency dispersion as a function of drive amplitude was measured before and after thermal conditioning to quantify α, the hysteretic nonlinearity of the PETN. This nonlinear parameter, α, was found to change with thermal conditioning and was well correlated with the post-conditioned explosives' initiation sensitivity. The nonlinear effect itself, however, is small and required considerable experimental effort to measure precisely due to careful alignment of a laser Doppler vibrometer that is used to measure resonances of the HE pellet and gluing of a piezo transducer directly to the pellet. Note also that the *nonlinear* resonant ultrasound technique used in this recent study provided quantification of the hysteretic nonlinearity of the PETN material but did not provide quantification of the HE bulk elastic properties that a *linear* RUS technique can provide.

Although *linear* RUS does not require such precise alignment or direct gluing of a piezo transducer to a sample, one drawback of linear RUS is that the inversion algorithm requires an initial guess of the material elastic stiffness coefficients and relatively simple object geometries, such as cylindrical and rectangular parallelepiped. Additionally, inconsistencies between the actual object geometry and the assumed shape as well as material inhomogeneities will manifest as errors in the elastic properties.[20] For simplicity, in this study, we assume the PETN-based materials to behave, on average, as linear, homogenous, and isotropic; therefore, two elastic stiffness coefficients are measured for each sample. The viability of assuming homogeneity for RUS measurements on macroscopic samples with mesoscopic inhomogeneity has been demonstrated previously,[21] given an adopted rule of thumb that the wavelength of the propagating ultrasonic wave is much greater than the length scale of inhomogeneity. For PETN-based materials, grain sizes are much smaller than 1 mm,[5,22] which is much less than the wavelength of ultrasound used for RUS measurements in this study (approximately a few mm).

Single crystal forms of HE materials, such as PETN, cyclotrimethylene trinitramine (RDX), and cyclotrimethylenete tranitramine (HMX), have tetragonal, orthorhombic, and monoclinic symmetry, respectively. The elastic properties of single crystal samples have already been characterized;[18] specifically, the full elastic tensor has been measured for PETN, RDX, and HMX using RUS and Brillouin scattering.[23–25] However, aside from the study of Stevens *et al.*[23] on single crystal PETN, we are unaware of studies investigating elastic properties in granular PETN and the feasibility of using RUS as a diagnostic for quantifying thermal conditioning related effects in PETN. Elastic properties measured by RUS could potentially be used to parameterize continuum simulation models, enabling comprehensive investigation of how these thermally induced changes couple with other material microstructural features (voids, gross aberrations, etc.), which further impact thermally induced changes to material performance.[26,27]

Ultimately, there is a need to demonstrate and develop non-destructive techniques that can characterize the mechanical properties of high explosive materials, particularly thermally conditioned materials, which could lead to better understanding of environmental aging-related effects (i.e., performance *and* safety). There is also an additional need for characterization techniques that can measure the mechanical properties of small high explosive samples, where using a traditional tool to generate a stress–strain curve to determine elastic properties may be less practical. Binderized PETN, typically used in detonators, is commonly used in small quantities and form factors. Thus, in this study, we demonstrate the first application of the RUS technique to not only quantify the elastic stiffness coefficients of pressed granular explosives, but also to characterize the effects of thermal conditioning on the elastic stiffness coefficients of binderized PETN and binderless, or "neat" PETN, particularly using small form factor samples. This is the first study of which we are aware to quantify elastic stiffness coefficients for high explosive pressings using RUS.

II. EXPERIMENTAL METHODS

A. PETN-based samples

In this study, binderized and neat PETN-based samples were measured in pre- and post-thermal conditions. The constituent PETN powder material was made at Pantex.[28] Readers interested in additional details about this material can also refer to the literature.[13,29] The PETN explosive pellets were all die pressed in cylindrical dies with different loading pressures depending upon the target pellet density. A loading pressure for a PETN pressing at 10 kpsi can typically result in a pressing density of 1.61 g/cm^3,[30] whereas a lower loading pressure of 5 kpsi can result in a density of 1.48 g/cm^3 and higher loading pressures would result in higher densities no more than the theoretical maximum density of PETN of 1.76 g/cm^3.[30]

The binderized samples were pressed into cylindrical pellets and had a composition of PETN with a few weight percent of an Oxy-461 polymeric binder, similar to that reported in other studies, such as Maiti *et al.*[5] We note that the few weight percent of an Oxy-461 polymer binder is similar to the 3–4 wt. % of an FPC-461 polymer binder commonly used in the previous literature.[29–32] The pellets had approximate densities, diameters, and lengths of 1.70 g/cm^3 or 1.56 g/cm^3, 0.635 cm, and 0.560 cm, respectively.

The neat PETN samples were also pressed into cylindrical pellets and are separated into two types, which are referred to in this study as Batch A and Batch B. There were some differences in the *input powder* used to fabricate the pellets in the two batches; for example, there was a higher surface area per unit mass (e.g., specific surface area) and greater thermal annealing for the powder used to fabricate the Batch B samples; annealing was performed for several hours in a drying oven (with no atmospheric controls) at a temperature well below the melting temperature of the material. Specific surface areas were measured on the constituent neat PETN powder materials using a commercially available flow permeametry instrument that has been customized.[33] More details about the

TABLE I. Summary of pre-T, post-T, and post-T + H conditions for the PETN-based samples.

Condition	Temperature (°C)	Pressure (atm)	Relative humidity (%)	Conditioning duration (days)	Gas species present
Pre-T	25 ± 5	1.0	20–50	N/A	Atmosphere
Post-T	80 ± 1	2.0	0–10	60	Nitrogen
Post-T + H	80 ± 1	1.0	25–35	60	Atmosphere

permeametry technique can be found in Ref. 33. Batch B neat PETN powder had specific surface area values similar to those commonly found in the literature for PETN powders before heat treatment, such as values reported in Lease *et al.*[10]

The neat PETN samples all had approximate densities, diameters, and lengths of 1.56 g/cm^3, 0.467 cm, and 0.233 cm, respectively. Mean densities for each sample batch are listed in the tables found later in this paper. Note, densities less than the theoretical maximum density reported for PETN pressings (1.76 g/cm^3 reported[30] and 1.768 g/cm^3 measured for a single PETN crystal[23]) correlate to the amount of porosity and spacing present between individual PETN crystals in the pressing.

The PETN-based samples in this study were thermally conditioned at temperatures and time durations similar to other studies, such as Schulze *et al.*[19] A summary of the thermal conditions for both the binderized and neat PETN pressings can be found in Table I. We note that the types of sample thermal conditioning will be referred to as either pre-T (pre-thermal conditioning), post-T (post-thermal conditioning), or post-T + H (post-thermal and humidity conditioning).

Physical measurements of each individual explosive pressing were averaged from three repeated measurements. The diameters and lengths of all explosive pressings were measured using a digital micrometer (Mitutoyo, 293-765-30) with 0.001 mm resolution. The mass of pressings was measured using a mass balance with 0.001 mg resolution. Pressing density was calculated from the measured mass and the calculated volume assuming the pressing was a right cylinder. The high explosive sample shape and plane parallelism of the cylindrical faces were ultimately controlled by the pressing die used during fabrication. Surface flatness was later characterized using commercial profilometers (Zygo Nexview and Zygo Zegage) confirming maximum surface variations on the order of 10 micrometers or less for the samples.

B. Resonant ultrasound spectroscopy measurement

For the RUS measurements in this study, a commercially available RUS system and analysis software (Alamo Creek Engineering, ACE-RUS008) was used. Details about the RUS system, the measurement technique, and the use of the analysis software can be found in the literature.[3,34,35] Briefly, the system setup includes two broadband transducers that make dry point contact with the pressed pellet sample to excite and detect mechanical resonances (or normal modes of vibration) of the sample. The samples were mounted between the two transducers with a minimal contact area and compression in order to best approximate a free-body resonator. One of the transducers provides sine wave excitation to the sample at a fixed frequency and the other transducer detects the in-phase and quadrature sample response with digital signal processing using a field-programmable gate array. The excitation is then stepped to the next frequency and eventually swept across a full frequency range of interest. In this study, all PETN-based pellets were measured from 20 to 900 kHz in 10 Hz steps, which ensured measurement of at least the first 30 resonant modes of the samples. The frequency spectra for each sample were measured twice consecutively at one mounted position, then the sample was remounted and reoriented between the transducers, and the frequency spectra were measured twice again. This was done to validate consistency of each measurement and maximize the excitation of as many resonant modes in the sample as possible.

C. Resonant ultrasound spectroscopy analysis

The RUS analysis software from Alamo Creek Engineering was used for post-processing and analysis. This includes a frequency peak fitting capability to find and quantify resonant modes in the measured RUS data using a complex Lorentzian function,[3]

$$Z(f) = \frac{Ae^{i\theta}}{f - f_0 + iB} + Z_{bg}, \tag{1}$$

where f is the frequency, A is the amplitude, θ is the phase, f_0 is the center frequency, B is the resonance half-width, and Z_{bg} is the background signal.

Before the measured resonant frequencies can be used to calculate the elastic properties of the explosive, a forward computation code was used to assist with properly ordering the measured resonant frequencies to match the expected resonant modes for the sample. The forward computation code computes the expected resonant frequencies for a right cylinder given the sample elastic moduli, mass, geometric dimensions, and order of symmetry in the material. Briefly, this forward computation involves finding solutions to the matrix eigenvalue problem for a freely vibrating elastic body that is derived starting from the linear elastic Lagrangian,[36,37]

$$\begin{aligned} L &= \int_V (E_K - E_P) dV \\ &= \int_V \left(\frac{1}{2} \sum_i \rho \omega^2 u_i^2 - \frac{1}{2} \sum_{i,j,k,l} c_{ijkl} \frac{\partial u_i}{\partial x_j} \frac{\partial u_k}{\partial x_l} \right) dV, \end{aligned} \tag{2}$$

where V is the object volume, E_K is the kinetic energy density, E_P is the potential energy density, ρ is the density, ω is the angular frequency, u_i is the ith component of the displacement vector, c_{ijkl} is the elastic stiffness tensor, and subscripts i, j, k, l refer to indices

in a Cartesian coordinate system. After expansion of the displacement field with the basis functions used by Visscher *et al.*,[2] derivation of when the Lagrangian is stationary, and exploiting symmetries of the problem, yields the following matrix eigenvalue problem:

$$\omega^2 \mathbf{E}\mathbf{a} = \mathbf{\Gamma}\mathbf{a}, \tag{3}$$

where matrix **E** comes from the kinetic energy term, **a** are the approximations to the motion expanded in a complete basis set, and matrix **Γ** comes from the elastic energy term.

The averaged measured mass, length, and diameter values were used in the forward computation code. The samples were assumed to have isotropic mechanical properties so only initial guesses for two elastic tensors components were required and were informed by values from contact pulse-echo measurements. The first 30 resonant modes were calculated using the forward model and were used to help guide the order of inputting the measured resonant modes into the inverse computation code. Note that it is generally recommended that a good fit needs approximately 15 non-pure shear modes for isotropic symmetry.[36] It was also particularly important to identify frequencies where degenerate modes occurred or where there were missed resonant modes that were not strongly excited within the sample.

For the inverse computation code, where elastic moduli are computed from the measured resonant modes, a numerical inversion is done using an iterative approach since there is no analytic inverse to the forward problem. This involves repeated applications of the forward computation where the elastic tensors components are varied until the computed resonant frequencies best match the measured resonant frequencies. The Levenberg–Marquardt minimization method[38] was followed to provide a nonlinear least-squares fit, where the following computed sum of weighted residuals is minimized:

$$F = \sum_{n=1}^{N} w_n (g_n - h_n)^2; \tag{4}$$

here, $\boldsymbol{g}$ and $\boldsymbol{h}$ are the vectors of measured and calculated frequencies, respectively, and w_n is a weighting factor chosen based on the confidence for the measurement of that mode frequency and is customarily set to unity for measured modes and 0 for missed modes. Figure 1 shows the RUS setup and how the resonant modes determined from the recorded spectrum can be used as an input for the inversion algorithm to calculate the elastic stiffness coefficients.

The complex Lorentzian function is fitted to the peak frequencies present in the recorded spectra to provide the eigenfrequencies, which are used to determine the elastic properties.[3] We note that the full-width-half-maximums for each resonance mode can also be quantified with this analysis, which could possibly be used to determine a quality factor and acoustic attenuation for each resonant mode. However, acoustic attenuation was determined to fall outside of the scope of this current work but will be considered in future analysis.

D. Contact pulse-echo ultrasound measurements

Pulse-echo ultrasound measurements were also performed on the binderized PETN samples for comparison with RUS measurements. A 0.25-in. diameter, 5 MHz center frequency longitudinal contact transducer (Olympus, V110-RM) and a shear contact transducer (Olympus, V156-RM) were used to determine longitudinal and shear wave speeds in each binderized PETN pressing, respectively. First, a thin layer of aged-honey (i.e., old viscous honey) was applied to each transducer face to be used as the acoustic couplant. Aged-honey was chosen for its ability to effectively couple both longitudinal and shear waves into the explosive pressing and for its confirmed chemical compatibility with PETN-based materials. A chemical reactivity test (CRT) was conducted internally to determine chemical compatibility between the HE material and the aged-honey couplant. More details about the CRT process can be found in the literature.[29,30] The binderized PETN pellet was then gently placed with its flat surface in contact with the transducer face. A pulse-echo measurement was made using a pulser-receiver (Panametrics, 5800), and each A-scan was digitized and recorded using an oscilloscope. The sample was then carefully transferred to the next contact transducer to record another A-scan. Afterward, the pellet was wiped clean of any visible residual aged-honey couplant using a cue tip wet with warm water. The time of flight for each recorded A-scan was determined by autocorrelation, and wave speeds were calculated using the measured sample length along the acoustic path. In this study, we assumed that our PETN-based

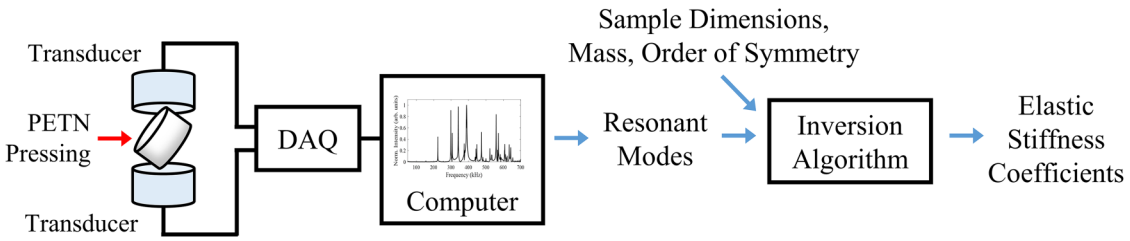

FIG. 1. An illustration of the RUS experimental setup and the analysis process. Recorded resonant modes are used along with sample diameter, length, mass, and order of symmetry as inputs to the inversion algorithm that calculates the elastic stiffness coefficients of the PETN pellet. Note that the forward computation is first used with estimated elastic stiffness coefficients to inform how the measured resonant modes are inputted into the inversion algorithm.

cylindrical pellets were linear, homogeneous, and isotropic. With these assumptions, Young's modulus, E, and Poisson's ratio, ν, can be calculated by

$$E = \frac{c_L^2 \rho (1+\nu)(1-2\nu)}{1-\nu}, \tag{5}$$

$$\nu = \frac{1-2(c_S/c_L)^2}{2-2(c_S/c_L)^2}, \tag{6}$$

where c_L is the longitudinal wave speed, c_S is the shear wave speed, and ρ is the density of the material.

III. RESULTS AND DISCUSSION

A. Comparing resonant ultrasound spectroscopy and contact ultrasound

RUS and contact ultrasound measurements were performed on four of the same binderized PETN samples. Table II shows the measured mean elastic stiffness coefficients for the pre-conditioned binderized PETN samples measured by contact pulse-echo and RUS. Examples of typical longitudinal and shear A-scans and the RUS spectrum for the same explosive pellet can be found in the supplementary material. Overall, the contact pulse-echo and RUS measured elastic constants are comparable and within 7.5% of each other.

An uncertainty analysis was also performed given the mean values of binderized PETN sample no. 1 for the bulk modulus, shear modulus, Young's modulus, and Poisson's ratio determined by a contact pulse-echo ultrasound. Here, we considered uncertainty in the measured height, diameter, mass, and time-of-flights of the longitudinal waves and shear waves. These uncertainties were propagated to the density, the longitudinal speed of sound, and the shear wave speed of sound and combined to determine the total uncertainty in each elastic constant. The elastic stiffness coefficients determined using this approach are for Young's modulus 8.62 ± 0.01 GPa, Poisson's ratio 0.273 ± 0.001, bulk modulus 6.32 ± 0.03 GPa, and shear modulus 3.39 ± 0.01 GPa. The density determined using this approach is 1.69 ± 0.01 g/cm^3. Uncertainties are reported in Table II.

Estimating error for individual elastic stiffness coefficients determined by RUS is challenging and has been proposed by calculating the curvature of the minimum solution to the inverse problem in parameter space.[34] Methods of uncertainty analysis for elastic stiffness coefficients determined by RUS have also been proposed in recent studies,[39–42] which have commonly involved finite element modeling and Monte Carlo analysis. Accurate estimation of error for RUS measurements deserves the attention of its own study and will be part of future investigation.

The RUS determined elastic stiffness coefficients are consistently greater than the contact pulse-echo coefficients; this may be due to the differences in which the two measurement techniques probe the material. RUS probes the entire sample with a broadband frequency to determine resonant modes, while the pulse-echo method probes only the sample volume along the path of the propagating waves and uses a much narrower band of frequency. Additionally, the wavelength of the ultrasound used by the pulse-echo method here is smaller by an order of magnitude than the wavelengths used by the RUS method, possibly making the pulse-echo method more susceptible to any inhomogeneities present on the same order of length scale as its wavelength.[21] Readers interested in further comparisons of pulse-echo contact measurements and RUS measurements can refer to additional literature.[23,43]

B. RUS of thermally conditioned binderized PETN samples at two different densities

Six binderized PETN samples were measured by RUS, and plots of their spectra are shown in Fig. 2. Two explosives of each thermal condition were also tested, where the explosives had nominal densities of either 1.70 g/cm^3 or 1.56 g/cm^3. Figure 2 shows the first few resonant modes for the pressings, and a clear shift to higher frequencies can be seen for all thermally conditioned samples compared to their respective pre-conditioned state. There is a greater frequency increase in the resonant modes for the lower density post- and pre-conditioned explosives. The red arrows in Fig. 2 highlight the resonant mode shifts from the pre- and post-conditioned spectra.

TABLE II. Summary of measured mean elastic stiffness coefficients for pre-conditioned binderized PETN pellets determined from pulse-echo contact ultrasound measurements and RUS measurements. Errors for the contact ultrasound values were calculated from uncertainty analysis and are reported in the table and text. Estimation of error for RUS measurements is more challenging and discussed further in the text.

Binderized PETN sample no.	Method	Density (g/cm^3)	Young's modulus (GPa)	Poisson's ratio	Bulk modulus (GPa)	Shear modulus (GPa)
1	Contact	1.69 ± 0.01	8.62 ± 0.01	0.273 ± 0.001	6.32 ± 0.03	3.39 ± 0.01
1	RUS	1.69 ± 0.01	8.92	0.281	6.78	3.48
2	Contact	1.69 ± 0.01	8.91 ± 0.01	0.274 ± 0.001	6.58 ± 0.03	3.50 ± 0.01
2	RUS	1.69 ± 0.01	9.17	0.278	6.89	3.59
3	Contact	1.71 ± 0.01	9.16 ± 0.01	0.287 ± 0.001	7.17 ± 0.03	3.56 ± 0.01
3	RUS	1.71 ± 0.01	9.56	0.289	7.54	3.71
4	Contact	1.71 ± 0.01	9.15 ± 0.01	0.287 ± 0.001	7.17 ± 0.03	3.55 ± 0.01
4	RUS	1.71 ± 0.01	9.45	0.294	7.66	3.65

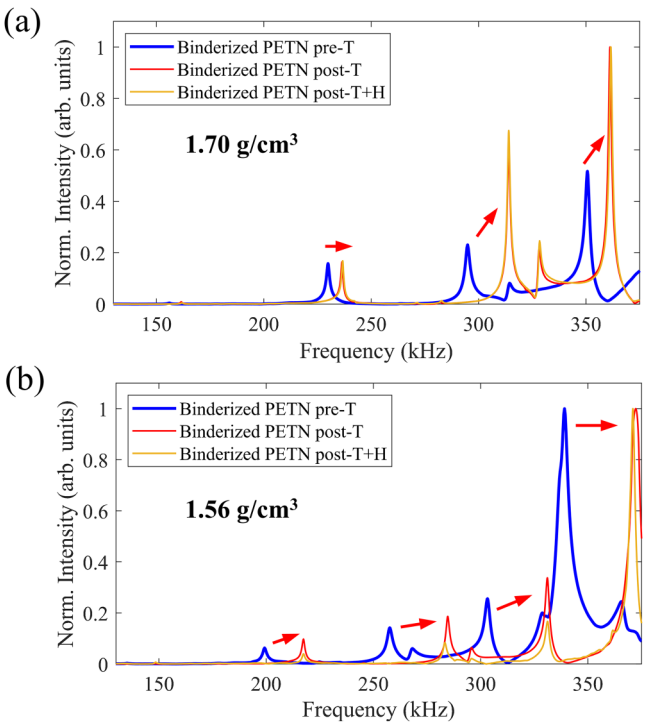

FIG. 2. Plot of the first few resonant modes for typical RUS spectra of (a) high-density (1.70 g/cm^3) binderized PETN pellets that are pre-T, post-T, and post-T + H and (b) lower density (1.56 g/cm^3) binderized PETN pellets that are pre-T, post-T, and post-T + H. Red arrows highlight pre-conditioned pellet resonant modes that shifted to higher frequencies for the post-conditioned pellets.

The derived elastic stiffness coefficients from the RUS measurements on the six binderized PETN samples are shown in Table III. Note that these are the mean values for each sample because each sample was measured twice at two different mounting orientations in the RUS setup. We find the elastic stiffness coefficients for the higher density pressings to be greater than those of the lower density. Additionally, there is a significant increase in the elastic stiffness coefficients from the pre- to post-conditioned pressings; for example, the average bulk modulus of the pre-T high-density sample was 28% greater than that of the corresponding post-T sample. The average bulk modulus increase was even greater for the low-density explosives where it increased by 58% between the post- and pre-conditioned pressings. Interestingly, there is not a large difference in elastic stiffness coefficients between the explosives thermally conditioned compared with explosives thermally conditioned with humidity.

C. RUS of thermally conditioned neat PETN pressings

Fifty-four neat PETN pressings were measured by RUS; typical plots of their spectra are shown in Fig. 3. Table IV provides the number of neat PETN Batch A and Batch B pressings measured at each thermal condition. Figure 3 shows the first few resonant modes for the pressings, and a clear shift to higher frequencies can be seen for the post-conditioned Batch A pressings compared to pre-conditioned pressing. The spectra for post-T and post-T + H explosives had resonant peaks at similar frequencies. The red arrows in Fig. 3 highlight the resonant mode shifts from the pre- to post-conditioned spectra. Interestingly, there is only a slight frequency shift for the post-T Batch B pressing compared to the pre-T pressing.

The elastic stiffness coefficients derived from RUS measurements on neat PETN pressings are shown in Table IV. Again, note that each sample was measured twice at two different mounting orientations in the RUS setup; hence, these are mean values. Similar to the binderized PETN pressings, there is a significant increase in elastic stiffness coefficients from the pre- to post-conditioning in the neat PETN pressings; for example, the average bulk modulus was greater by 65% for post-conditioned Batch A compared to pre-conditioned Batch A. However, the average bulk modulus increase was much less for the neat PETN Batch B where it increased by only 15% between the post- and pre-conditioned pressings. Similar to the results from the binderized PETN, there is not a large difference in elastic stiffness coefficients between the post-T samples and the post-T + H samples.

Additionally, the differences between the average elastic stiffness coefficients for post-T neat PETN Batch A and Batch B are much less than the differences between the unconditioned Batch A and Batch B elastic stiffness coefficients; for example, the difference between the average bulk modulus for the pre-conditioned neat

TABLE III. Summary of the elastic stiffness coefficients and densities (mean ± standard deviation) for binderized PETN pre-T, post-T, and post-T + H determined from RUS measurements. The percentage difference between the mean values for the post-conditioned and corresponding pre-conditioned HE samples is shown in parentheses. Note that only one binderized PETN sample was measured for each thermal condition and density.

Binderized PETN condition	Density (g/cm^3)	Young's modulus (GPa)	Poisson's ratio	Bulk modulus (GPa)	Shear modulus (GPa)
Pre-T	1.68 ± 0.01	8.84 ± 0.03	0.274 ± 0.007	6.53 ± 0.23	3.47 ± 0.01
Post-T	1.69 ± 0.01	9.65 ± 0.01 (+9%)	0.297 ± 0.001 (+8%)	7.92 ± 0.04 (+21%)	3.72 ± 0.01 (+7%)
Post-T + H	1.69 ± 0.01	9.68 ± 0.01 (+10%)	0.306 ± 0.002 (+12%)	8.33 ± 0.09 (+28%)	3.71 ± 0.01 (+7%)
Pre-T	1.55 ± 0.01	5.72 ± 0.01	0.180 ± 0.003	2.98 ± 0.02	2.42 ± 0.01
Post-T	1.56 ± 0.01	7.11 ± 0.02 (+24%)	0.228 ± 0.011 (+27%)	4.35 ± 0.18 (+46%)	2.89 ± 0.02 (+19%)
Post-T + H	1.55 ± 0.01	7.15 ± 0.02 (+25%)	0.247 ± 0.011 (+37%)	4.71 ± 0.23 (+58%)	2.87 ± 0.02 (+19%)

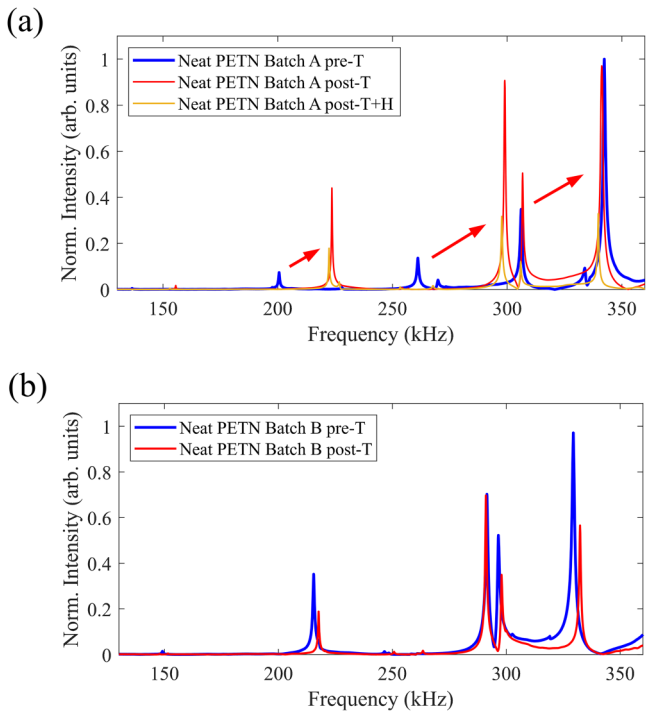

FIG. 3. Plot of the first few resonant modes for typical RUS spectra of (a) neat PETN Batch A pellets that are pre-T, post-T, and post-T + H and (b) neat PETN Batch B pellets that are pre-T and post-T. Red arrows highlight pre-conditioned pellet resonant modes that shifted to higher frequencies for the post-conditioned pellets. Note that the frequency shift for Batch B spectra was not very large; therefore, red arrows were not added to plot in (b). Also note that the highest frequency resonant modes in part (a) for the post-T and post-T + H Batch A spectra have shifted outside of the frequency window shown. Differences seen between Batch A and Batch B are discussed further in Sec. III C.

PETN Batch A and Batch B was 1.12 GPa, while this difference was only 0.59 GPa for the post-T Batch A and Batch B. This could possibly suggest that although neat PETN pellets have different starting elastic properties, these differences may be minimized after thermal conditioning. Also, the smaller absolute change of elastic properties for Batch B compared to Batch A may be due to the Batch B input powder having undergone greater thermal annealing before pressing. This could possibly suggest that changes from thermal conditioning may differ and depend upon the pre-conditioned state and elastic properties of the PETN pellets. Figures 4(a)–4(c) show box plots of the elastic stiffness coefficients values for the neat PETN pressings derived from RUS measurements. Statistical significance between the pre- and post-conditioned elastic properties is verified and detailed later in this section.

D. Elastic property changes due to thermal conditioning are independent of density

Figure 4(d) shows a box plot of the bulk densities for the neat PETN pressings derived from measurements of mass and physical dimensions. The density differences between the pre- and post-conditioned groups (less than ~2.5%) seen in Fig. 4(d) do not correlate with the changes seen in elastic stiffness coefficients [Figs. 4(a)–4(c)]. Thus, the changes in elastic properties measured by RUS are not density-related changes, but rather due to thermal conditioning related effects of the neat PETN samples, possibly powder coarsening due to sintering and mass transport.[6,9,10] This agrees well with the understanding that ultrasonic waves are known to be sensitive to changes in the specific surface area of powder compacts that have undergone solid-state sintering.[44–46] For additional reference, the theoretical maximum density of a neat PETN pressing would be the density of a single PETN crystal, 1.76 g/cm^3,[30] which has a reported Voigt approximated bulk modulus of 8.63 GPa and a shear modulus of 4.42 GPa measured by RUS.[23]

It is important to note that explosive particle coarsening due to thermal conditioning effects studied in the literature has typically been monitored using microscopy and flow permeametry characterization techniques that either require the HE material to be in a free powder form or pressed to a very low density close to 0.5 porosity, whereas as we have shown in this study, the RUS technique is able to probe HE pellets at higher bulk pressing densities that are closer to the theoretical maximum density for PETN, which is 1.76 g/cm^3.[30] Thus, this demonstrates the possibility of using RUS as a non-destructive characterization tool for monitoring explosive particle coarsening effects in high-density pressings where other characterization techniques are no longer possible. However, an accurate correlation between RUS determined elastic property changes and microstructural changes in a granular HE pressing after thermal conditioning deserves a separate study and falls outside of the scope for this work.

TABLE IV. Summary of the elastic stiffness coefficients and densities (mean ± standard deviation) for neat PETN Batch A pressings pre-T, post-T, and post-T + H and neat PETN Batch B pressings pre-T and post-T determined from RUS measurements. The percentage difference between the mean values for the post-conditioned and corresponding pre-conditioned HE samples is shown in parentheses.

Neat PETN samples	Condition	Number of samples	Density (g/cm^3)	Young's modulus (GPa)	Poisson's ratio	Bulk modulus (GPa)	Shear modulus (GPa)
Batch A	Pre-T	11	1.58 ± 0.01	6.10 ± 0.19	0.225 ± 0.017	3.71 ± 0.30	2.49 ± 0.07
Batch A	Post-T	10	1.58 ± 0.01	7.91 ± 0.08 (+30%)	0.285 ± 0.006 (+27%)	6.13 ± 0.19 (+65%)	3.08 ± 0.03 (+24%)
Batch A	Post-T + H	10	1.56 ± 0.01	7.83 ± 0.11 (+28%)	0.287 ± 0.004 (+28%)	6.13 ± 0.17 (+65%)	3.04 ± 0.04 (+22%)
Batch B	Pre-T	10	1.57 ± 0.01	7.15 ± 0.10	0.253 ± 0.008	4.83 ± 0.16	2.86 ± 0.04
Batch B	Post-T	13	1.57 ± 0.01	7.55 ± 0.14 (+6%)	0.272 ± 0.010 (+8%)	5.54 ± 0.33 (+15%)	2.97 ± 0.04 (+4%)

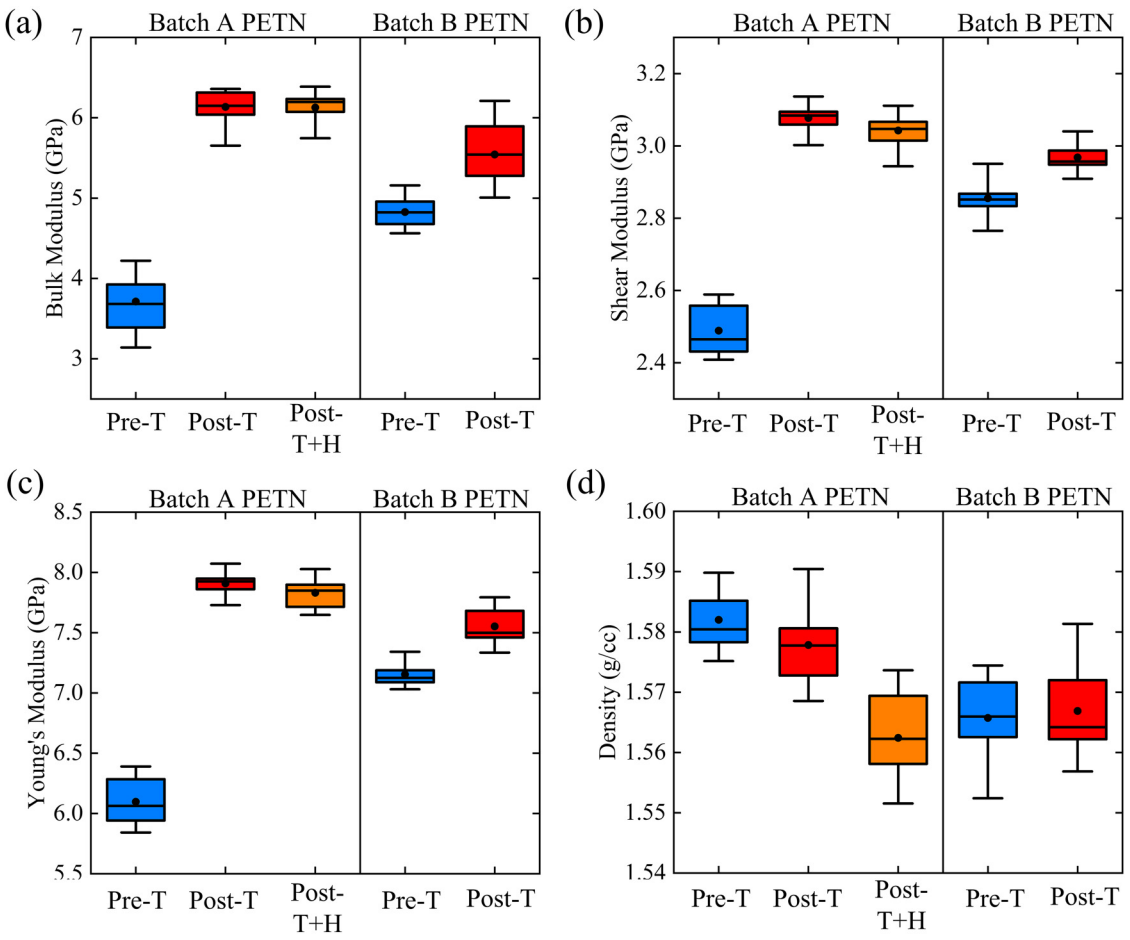

FIG. 4. Box plots of (a) bulk moduli, (b) shear moduli, and (c) Young's moduli for pre- and post-conditioned neat PETN Batch A and Batch B pressings determined from RUS measurement. (d) Box plot of the calculated densities for pre- and post-conditioned Batch A and Batch B pressings. The boxes mark the first, second, and third quartiles, the whiskers show the maximum and minimums, and the mean value is identified by the black circle marker.

E. Statistical significance testing for changes with thermal conditioning

A Shapiro–Wilk test for normality ($p < 0.05$) showed that the elastic stiffness coefficients for each type of sample were not all normally distributed; therefore, nonparametric statistical testing was conducted using OriginPro software. The Mann–Whitney *U* test showed that the elastic stiffness coefficients for all post-T and post-T + H neat PETN samples were significantly greater than the corresponding pre-T samples ($p < 0.01$). Additionally, statistical testing found significant differences for Young's moduli and shear moduli between the post-T and post-T + H neat PETN Batch A samples, possibly indicating that thermal conditioning with humidity could be affecting these elastic properties for neat PETN Batch A pressings to some degree. However, no significant differences were found between the bulk moduli and Poisson's ratios for the post-T and post-T + H samples. Also, significant differences were not found between the bulk densities of the pre- and post-conditioned neat PETN pressings for both Batch A and Batch B types, reaffirming that the measured elastic property changes are not due to density changes. Interestingly, the elastic stiffness coefficients for the pre-T Batch B type were found to be significantly greater than ($p < 0.01$) than that of the pre-T Batch A type due to possible differences in crystal size, crystal shape, or thermal histories of their constituent powders.

IV. CONCLUSION

We demonstrate RUS as a suitable non-destructive characterization technique for quantifying HE elastic stiffness coefficients and measuring thermal conditioning related effects for binderized and neat PETN-based pressed powders. We show agreement between RUS and conventional contact pulse-echo ultrasound measurements on the same pre-conditioned binderized PETN pressings. A consistent overall trend of increased elastic stiffness coefficients with thermal conditioning was measured with RUS.

The change in elastic properties, due to thermal conditioning, was consistent for the different bulk density binderized PETN samples and the two different neat PETN pressing types. Additionally, minor differences were found between Young's moduli and shear moduli of the two differently thermally conditioned neat PETN Batch A pressings (one conditioned with humidity). The RUS measured effects of thermal conditioning on the elastic stiffness coefficients for PETN-based materials may be extendable to other high explosive materials and help provide valuable insights into material changes of thermally conditioned high explosives in the future.

SUPPLEMENTARY MATERIAL

See the supplementary material for details of considerations taken for experimental measurements and assumptions used in this study.

ACKNOWLEDGMENTS

This work was performed under the auspices of the U.S. Department of Energy by Lawrence Livermore National Laboratory under Contract No. DE-AC52-07NA27344. The LLNL document release number is LLNL-JRNL-857874.

AUTHOR DECLARATIONS

Conflict of Interest

The authors have no conflicts to disclose.

Author Contributions

Jordan S. Lum: Conceptualization (equal); Formal analysis (equal); Investigation (equal); Writing – original draft (equal); Writing – review & editing (equal). **David M. Stobbe:** Conceptualization (equal); Formal analysis (equal); Investigation (equal); Writing – original draft (equal); Writing – review & editing (equal). **Paul B. Mirkarimi:** Conceptualization (equal); Formal analysis (equal); Investigation (equal); Writing – original draft (equal); Writing – review & editing (equal). **William L. Shaw:** Conceptualization (equal); Data curation (equal); Investigation (equal); Resources (equal); Writing – review & editing (equal). **Henry E. Reinstein:** Data curation (equal); Resources (equal); Writing – review & editing (equal). **Rebecca K Lindsey:** Formal analysis (equal); Resources (equal); Writing – original draft (equal); Writing – review & editing (equal). **Richard H. Gee:** Conceptualization (equal); Funding acquisition (lead); Investigation (equal); Resources (equal); Writing – review & editing (equal).

DATA AVAILABILITY

The data that support the findings of this study are available within the article and its supplementary material.

REFERENCES

[1]A. Migliori, J. L. Sarrao, W. M. Visscher, T. M. Bell, M. Lei, Z. Fisk, and R. G. Leisure, "Resonant ultrasound spectroscopic techniques for measurement of the elastic moduli of solids," Phys. B: Condens. Matter **183**, 1–24 (1993).

[2]W. M. Visscher, A. Migliori, T. M. Bell, and R. A. Reinert, "On the normal modes of free vibration of inhomogeneous and anisotropic elastic objects," J. Acoust. Soc. Am. **90**, 2154–2162 (1991).

[3]F. F. Balakirev, S. M. Ennaceur, R. J. Migliori, B. Maiorov, and A. Migliori, "Resonant ultrasound spectroscopy: The essential toolbox," Rev. Sci. Instrum. **90**, 121401 (2019).

[4]S. Meyers and E. S. Shanley, "Industrial explosives—A brief history of their development and use," J. Hazard. Mater. **23**, 183–201 (1990).

[5]A. Maiti *et al.*, "Topological analysis of x-ray CT data for the recognition and trending of subtle changes in microstructure under material aging," Comput. Mater. Sci. **182**, 109782 (2020).

[6]A. Maiti, T. Y. Olson, T. Y. Han, and R. H. Gee, "Long-term coarsening and function-time evolution of an initiator powder," Propellants Explos. Pyrotech. **42**, 1352–1357 (2017).

[7]A. Maiti and R. H. Gee, "PETN coarsening—Predictions from accelerated aging data," Propellants Explos. Pyrotech. **36**, 125–130 (2011).

[8]J. Rogers and A. A. Duncan, "Effects of particle characteristics on performance of RR5K PETN," No. SAND-81-2199, Sandia National Laboratories (SNL-NM), Albuquerque, NM; Mason & Hanger-Silas Mason Co., Inc., Amarillo, TX, 1982; see https://www.osti.gov/biblio/5251499.

[9]A. Maiti and R. H. Gee, "Modeling growth, surface kinetics, and morphology evolution in PETN," Propellants Explos. Pyrotech. **34**, 489–497 (2009).

[10]N. Lease *et al.*, "The role of pentaerythritol tetranitrate (PETN) aging in determining detonator firing characteristics," Propellants Explos. Pyrotech. **46**, 26–38 (2021).

[11]M. F. Foltz, "Aging of pentaerythritol tetranitrate (PETN)," No. LLNL-TR-415057, Lawrence Livermore National Laboratories (LLNL), Livermore, CA, 2009; see https://www.osti.gov/biblio/966904.

[12]R. H. Dinegar, "The effect of heat on pentaerythritol tetranitrate (PETN)," in *Proceedings of the 12th International Pyrotechnics Seminar*, Juan-Les-Pins, France (1987).

[13]A. A. Duncan, "Effects of various environmental conditions on recrystallized PETN," No. MHSMP-72-31, Mason & Hanger-Silas Mason Co., Inc., Amarillo, TX, Texas Development Division, 1972; see https://www.osti.gov/biblio/4631753.

[14]S. K. Bhattacharia, A. Maiti, R. H. Gee, J. Nunley, and B. L. Weeks, "Effect of homolog doping on surface morphology and mass-loss rates from PETN crystals: Studies using atomic force microscope and thermogravimetric analysis," Propellants Explos. Pyrotech. **39**, 24–29 (2014).

[15]L. A. Zepeda-Ruiz, G. H. Gilmer, A. Maiti, R. H. Gee, and A. K. Burnham, "Evaporation from the (110) surface of PETN," J. Cryst. Growth **310**, 3812–3819 (2008).

[16]G. Zhang, B. Weeks, R. Gee, and A. Maiti, "Fractal growth in organic thin films: Experiments and modeling," Appl. Phys. Lett. **95**, 204101 (2009).

[17]G. W. Brown, M. M. Sandstrom, A. M. Giambra, J. G. Archuleta, and D. C. Monroe, "Understanding aging in pentaerythritol tetranitrate," No. LA-UR-09-03972, Los Alamos National Laboratories (LANL), Los Alamos, NM, 2009; see https://www.osti.gov/biblio/990308.

[18]D. E. Hooks, K. J. Ramos, C. A. Bolme, and M. J. Cawkwell, "Elasticity of crystalline molecular explosives," Propellants Explos. Pyrotech. **40**, 333–350 (2015).

[19]P. Schulze, E. Pittman, S. Sjue, D. S. Moore, T. Feagin, and C. Donahue, "Nonlinear resonant ultrasound spectroscopy for predicting sensitivity to initiation in granular high explosives," Propellants Explos. Pyrotech. **45**, 387–395 (2020).

[20]B. J. Zadler, *Properties of Elastic Materials Using Contacting and Non-Contacting Acoustic Spectroscopy* (Colorado School of Mines, 2005).

[21]T. J. Ulrich, K. R. McCall, and R. A. Guyer, "Determination of elastic moduli of rock samples using resonant ultrasound spectroscopy," J. Acoust. Soc. Am. **111**, 1667–1674 (2002).

[22]G. D. Kosiba, H. K. Springer, W. L. Shaw, and R. H. Gee, "Determining shock response of PETN-based explosives with grain-scale simulations," AIP Conf. Proc. **2272**, 070022 (2020).

[23]L. L. Stevens, D. E. Hooks, and A. Migliori, "A comparative evaluation of elasticity in pentaerythritol tetranitrate using Brillouin scattering and resonant ultrasound spectroscopy," J. Appl. Phys. **108**, 053512 (2010).

[24]R. B. Schwarz, D. E. Hooks, J. J. Dick, J. I. Archuleta, and A. R. Martinez, "Resonant ultrasound spectroscopy measurement of the elastic constants of cyclotrimethylene trinitramine," J. Appl. Phys. **98**, 056106 (2005).
[25]L. L. Stevens and C. J. Eckhardt, "The elastic constants and related properties of β-HMX determined by Brillouin scattering," J. Chem. Phys. **122**, 174701 (2005).
[26]E. L. Lee and C. M. Tarver, "Phenomenological model of shock initiation in heterogeneous explosives," Phys. Fluids **23**, 2362–2372 (1980).
[27]C. Tarver, "Jones–Wilkins–Lee unreacted and reaction product equations of state for overdriven detonations in octogen- and triaminotrinitrobenzene-based plastic-bonded explosives," J. Phys. Chem. A **124**, 1399–1408 (2020).
[28]A. G. Osborn, HE formulation, quarterly report, January–March, 1968, No. MHSMP-68-1E, Mason & Hanger-Silas Mason Co., Inc., Amarillo, TX, 1968; see https://www.osti.gov/biblio/527452.
[29]M. F. Foltz, P. Reyes, and P. A. Foster, "CRT compatibility evaluation of LX-16 and Halthane 73-18," No. UCRL-JC-133765-Rev-1; DP0401281, Lawrence Livermore National Laboratories (LLNL), Livermore, CA, 1999; see https://www.osti.gov/biblio/14484.
[30]P. W. Cooper, *Explosives Engineering* (Wiley-VCH, 1996).
[31]M. Szala, "Polymer-bonded secondary explosives," Mater. Wysokoenergetyczne **T. 13**, 5-16 (2021).
[32]K. T. Lorenz, E. L. Lee, and R. Chambers, "A simple and rapid evaluation of explosive performance—The disc acceleration experiment," Propellants Explos. Pyrotech. **40**, 95–108 (2015).
[33]A. Maiti, Y. Han, F. Zaka, and R. H. Gee, "In-situ monitoring of flow-permeable surface area of high explosive powder using small sample masses," Propellants Explos. Pyrotech. **40**, 419–425 (2015).
[34]A. Migliori and J. L. Sarrao, *Resonant Ultrasound Spectroscopy Applications to Physics, Materials Measurements, and Nondestructive Evaluation*, 1st ed. (Wiley-VCH, New York, 1997).
[35]A. Balodhi, K. Chang, K. T. Stevens, S. K. Chakrapani, S. M. Ennaceur, A. Migliori, and A. Zevalkink, "Determination of single crystal elastic moduli of KTb3F10 by resonant ultrasound spectroscopy," J. Appl. Phys. **128**, 165104 (2020).
[36]A. Migliori and J. D. Maynard, "Implementation of a modern resonant ultrasound spectroscopy system for the measurement of the elastic moduli of small solid specimens," Rev. Sci. Instrum. **76**, 121301 (2005).
[37]H. H. Demarest, "Cube-resonance method to determine the elastic constants of solids," J. Acoust. Soc. Am. **49**, 768–775 (1971).
[38]K. Levenberg, "A method in the solution of certain non-linear problems in least squares," Q. Appl. Math. **2**, 164 (1944).
[39]J. C. Aldrin, A. Mayes, L. Jauriqui, E. Biedermann, J. Heffernan, R. Livings, B. Goodlet, and S. Mazdiyasni, "Uncertainty quantification of resonant ultrasound spectroscopy for material property and single crystal orientation estimation on a complex part," AIP Conf. Proc. **1949**, 140010 (2018).
[40]E. Biedermann, L. Jauriqui, J. C. Aldrin, A. Mayes, T. Williams, and S. Mazdiyasni, "Uncertainty quantification in modeling and measuring components with resonant ultrasound spectroscopy," AIP Conf. Proc. **1706**, 070008 (2016).
[41]B. Bales, L. Petzold, B. R. Goodlet, W. C. Lenthe, and T. M. Pollock, "Bayesian inference of elastic properties with resonant ultrasound spectroscopy," J. Acoust. Soc. Am. **143**, 71–83 (2018).
[42]S. Bernard, G. Marrelec, P. Laugier, and Q. Grimal, "Bayesian normal modes identification and estimation of elastic coefficients in resonant ultrasound spectroscopy," Inverse Probl. **31**, 065010 (2015).
[43]M. C. Remillieux, T. J. Ulrich, C. Payan, J. Rivière, C. R. Lake, and P.-Y. Le Bas, "Resonant ultrasound spectroscopy for materials with high damping and samples of arbitrary geometry," J. Geophys. Res. Solid Earth **120**, 4898–4916 (2015).
[44]E. P. Papadakis, "Determination of powder metal density by ultrasonic velocity," in *1976 Ultrasonics Symposium* (IEEE, 1976), pp. 133–137.
[45]V. J. García and C. H. Schilling, "Ultrasonic velocity and reduction of surface area during solid-state sintering," Mater. Sci. Eng. A **265**, 42–49 (1999).
[46]L. P. Martin and M. Rosen, "Correlation between surface area reduction and ultrasonic velocity in sintered zinc oxide powders," J. Am. Ceram. Soc. **80**, 839–846 (1997).